Original Article

# Identification of a C2H2 zinc finger-related lncRNA prognostic signature and its association with the immune microenvironment in clear cell renal cell carcinoma

**Ting Tian[1#], Cheng Shen[2,3#], Łukasz Zapała[4], Xingxing Fang[5], Bing Zheng[2,3]**

[1]Operating Room Nursing, The Second Affiliated Hospital of Nantong University, Nantong, China; [2]Department of Urology, The Second Affiliated Hospital of Nantong University, Nantong, China; [3]Jiangsu Nantong Urological Clinical Medical Center, Nantong, China; [4]Clinic of General, Oncological and Functional Urology, Medical University of Warsaw, Warsaw, Poland; [5]Department of Nephrology, Affiliated Hospital 2 of Nantong University, Nantong, China

*Contributions:* (I) Conception and design: T Tian, C Shen; (II) Administrative support: X Fang, B Zheng; (III) Provision of study materials or patients: X Fang, B Zheng; (IV) Collection and assembly of data: C Shen; (V) Data analysis and interpretation: T Tian; (VI) Manuscript writing: All authors; (VII) Final approval of manuscript: All authors.

[#]These authors contributed equally to this work.

*Correspondence to:* Xingxing Fang, PhD. Department of Nephrology, Affiliated Hospital 2 of Nantong University, 666 Shengli Road, Chongchuan District, Nantong 226001, China. Email: 48776592@qq.com; Bing Zheng, PhD. Department of Urology, The Second Affiliated Hospital of Nantong University, 666 Shengli Road, Chongchuan District, Nantong 226001, China; Jiangsu Nantong Urological Clinical Medical Center, Nantong, China. Email: ntzb2008@163.com.

**Background:** Clear cell renal cell carcinoma (ccRCC) is the main component of renal cell carcinoma, and advanced ccRCC often predicts a poor prognosis. In recent years, research has revealed the critical role of Cys2His2 zinc finger genes (CHZFs) and long non-coding RNAs (lncRNAs) in the development of cancer. Currently, little is known about the prognostic value of the lncRNAs linked to Cys2His2 (C2H2) zinc finger proteins (ZFPs) in ccRCC. The aim of this study was to construct a prognostic model for C2H2-associated lncRNAs to assist in the selection of clinical therapy.

**Methods:** RNA-sequencing data, and related clinical and prognostic information were downloaded from The Cancer Genome Atlas (TCGA) database. Univariate and multivariate Cox regression analyses were conducted to identify Cys2His2 zinc finger-associated long non-coding RNAs (CHZFLs) and build prediction signatures. A receiver operating characteristic (ROC) curve analysis was performed to validate the risk model. The prognosis of the groups was analyzed using the Kaplan-Meier method. The independent prognostic significance of these signatures was evaluated by univariate and multivariate Cox regression analyses. The relationship between the CHZFL signature and ccRCC tumor immunity was confirmed by a differential analysis of immune function and immunological checkpoints.

**Results:** A signature composed of five lncRNAs (AL117336.2, AC026401.3, AC124854.1, DBH-AS1, and LINC02100) was constructed. The results revealed a strong correlation between the CHZFLs signature and the prognosis of ccRCC patients. Prognostic characteristics of CHZFLs are independent prognostic factors in ccRCC patients. The diagnostic efficacy of the predictive signature was higher than that of individual clinicopathologic variables, and it had a ROC area under the curve (AUC) of 0.775. The results of the clinical subgroup analysis showed that the high-risk group had shorter overall survival (OS) than the low-risk group. Common chemotherapy medications, including vinorelbine, cytarabine, epirubicin, and gemcitabine, caused increased sensitivity in the high-risk group. Additionally, the single-sample gene set enrichment analysis (ssGSEA) revealed that the immunological state of the ccRCC patients was substantially linked with the predictive parameters.

**Conclusions:** The five CHZFL signature can help predict the prognosis of ccRCC patients, and assist in selecting immunotherapy and chemotherapy regimens in clinical practice.

**Keywords:** Immune infiltration; Cys2His2 zinc finger (C2H2 zinc finger); long non-coding RNAs (lncRNAs); clear cell renal cell carcinoma (ccRCC)

Submitted Dec 26, 2024. Accepted for publication Jan 22, 2025. Published online Feb 25, 2025.
doi: 10.21037/tau-2024-769
**View this article at:** https://dx.doi.org/10.21037/tau-2024-769

## Introduction

Renal cell carcinoma (RCC) is the most common cancer of the urinary system, and is increasingly characterized by high-grade tumors, often diagnosed at advanced stages (1,2). Based on morphology, RCC can be roughly divided into three subgroups: kidney renal clear cell carcinoma (KIRC), kidney renal papillary cell carcinoma (KIRP), and suspected cellular malignancies (3). More than 70% of RCC cases are KIRC (4). Even with advances in RCC diagnosis, screening, surgery, and drug therapy, patients with metastatic clear cell renal cell carcinoma (ccRCC) have a 5-year overall survival (OS) rate of about 12% (5-7). Immune checkpoint inhibitors (ICIs), which include anti-programmed death-1 (PD-1)/programmed death-ligand 1 (PD-L1) antibodies, are the most recent therapeutic approach, and have been gradually incorporated into clinical practice (8,9). However, some individuals do not respond well to ICIs, and serious side effects of the immunotherapy is often reported (10-12). For this reason, the course and prognosis of ccRCC depend heavily on the search for biomarkers and novel potential target medications.

One of the proteins found in the most significant quantity in eukaryotic genomes are zinc finger proteins (ZFPs). ZFPs have many diverse roles, including those related to genome recognition, RNA packing, transcription activation, apoptotic regulation, protein folding and assembly, and lipid binding (13). A study has examined Cys2His2 (C2H2) type ZFPs, which can precisely identify target sites in chromosomes and successfully control the expression of their target genes (14). An increasing body of research indicates that the aberrant expression of C2H2-type ZFPs contributes to the development of numerous cancers, including lung, prostate, and colorectal cancers (15-18). Transcription factors (TFs), particularly C2H2-type ZFPs, have recently been identified as prospective anti-cancer targets (19). Salidroside, a promising anti-cancer medication used to treat hematological malignancies, targets TFs and inhibits ZFPs (20,21). ZNF692 activates the mitogen-activated protein kinase kinase (MEK)/extracellular signal-regulated kinases (ERK) pathway via tyrosine kinase non receptor 2 (TNK2) to increase osteosarcoma cell motility, invasion, and proliferation (22). In addition, severe atopic illness and immunological dysregulation are caused by mutations in the C2H2 zinc finger TF BCL11B (23). According to research by Chu *et al.* (24), ZNF706 is a C2H2-type ZFP that functions as an oncogene and an iron-death modulator in liver cancer by controlling the

### Highlight box

**Key findings**

- Using data from The Cancer Genome Atlas database, five Cys2His2 zinc finger-associated long non-coding RNAs (CHZFLs) (AL117336.2, AC026401.3, AC124854.1, DBH-AS1, and LINC02100) were selected to construct clear cell renal cell carcinoma (ccRCC) prognostic characteristic models. A risk-score formula was established, and is expressed as follows: risk score = 0.654 × AL117336.2 expression + 0.315 × AC026401.3 expression − 0.380 × AC124854.1 expression + 0.269 × DBH-AS1 expression + 0.256 × LINC02100 expression.
- The model effectively predicted the prognosis of ccRCC patients, with patients in the high-risk group had shorter overall survival than those in the low-risk group. The immunological analysis showed that immune status was associated with the model. Patients in the high-risk group were more sensitive to some chemotherapeutic agents, while those in the low-risk group were more sensitive to other chemotherapeutic agents.

**What is known and what is new?**

- Cys2His2 zinc finger proteins and CHZFLs are known to play an important role in the development of cancer, but research on the association between the two in ccRCC is limited.
- The five newly discovered CHZFLs can be used to construct prognostic models, and are related to the immune microenvironment and chemosensitivity.

**What is the implication, and what should change now?**

- Our findings can help clinicians to better predict the prognosis of ccRCC patients, establish personalized treatment regimens, and select more appropriate immunotherapy and chemotherapy regimens.
- Future studies should seek to further validate the model using external datasets, conduct *in vitro* and *in vivo* experiments to identify long non-coding RNA function.

expression of SLC7A11. Thus, ZNF706 is a viable target for liver cancer therapy.

Non-protein-coding RNA with a length of more than 200 nucleotides is referred to as long non-coding RNA (lncRNA) (25). LncRNA has been widely shown to play a critical regulatory role in the development of cancer and numerous other disease processes (26). The advancement of RCC can be accelerated by lncRNA (SNHG1) via sponging microRNA (miR)-103a to mediate HMGA2 (27). Through the competing endogenous-mediated signaling pathway, HILAR can increase the spread of RCC (28). Siglec-15, which is implicated in the immunological escape response of ccRCC, is positively regulated by LINC00973 (29). However, to date, few studies have been conducted on the lncRNAs associated with the C2H2 zinc fingers, and the Cys2His2 zinc finger-associated long non-coding RNAs (CHZFLs) in ccRCC have not yet been identified.

In this study, we developed a predictive signature based on five CHZFLs, verified the accuracy of the model using various datasets, and then analyzed and evaluated the utility of the signature in predicting the prognosis, systemic treatment response, and pathological response, including tumor immune infiltration of ccRCC patients. We present this article in accordance with the TRIPOD reporting checklist (available at https://tau.amegroups.com/article/view/10.21037/tau-2024-769/rc).

## Methods

### *Acquisition and processing of data*

Associated clinical and prognostic KIRC data, the survival time data of 613 patients, and RNA-sequencing results normalized to fragments per kilobase million (FPKM) were downloaded from The Cancer Genome Atlas (TCGA) database (https://portal.gdc.cancer.gov/). To be eligible for inclusion in the study, the patients had to have been followed up for more than 30 days. Because more patients lacked lymph node metastasis data, we did not analyze information on lymph node status. Ultimately, the data of 507 patients were included in the study. All ccRCC patients with missing OS or clinical data were excluded from this study. We first identify batch effects by DESeq2 and principle component analysis (PCA) analysis, and then use the ComBat function of the sva package with DESeq2 to eliminate batch effects. The patients were randomly assigned to the training group (n=255) and the test group (n=252) at a ratio of 1:1. The basic characteristics of the studied cohort were presented in *Table 1*. Disease-free survival (DFS) data for 111 KIRC patients were downloaded from the cBioPortal database (https://www.cbioportal.org/). A total of 846 Cys2His2 zinc finger genes (CHZFs) with a relevance score ≥7 were extracted from GeneCards (https://www.genecards.org/) (available online: https://cdn.amegroups.cn/static/public/tau-2024-769-1.xls). Using previously described methodologies, the limma program was used to select the differentially expressed CHZFs that met the following criteria: a false discovery rate (FDR) <0.05, and a |a log2 fold change (FC)| ≥1 (30).

The study was conducted in accordance with the Declaration of Helsinki (as revised in 2013).

### *Functional enrichment analysis*

"Ggplot2" software was used to analyze data from the Gene Ontology (GO) and Kyoto Encyclopedia of Genes and Genomes (KEGG) databases. To investigate the biological role of these lncRNAs in ccRCC, we found messenger RNAs (mRNAs) that were highly connected to the five lncRNAs previously described. Five lncRNA-mRNA co-expression networks were created and depicted using Sanky diagrams. A P value <0.001 was considered statistically significant in both scenarios, with the correlation coefficient criterion set at either >0.4 or <0.4.

### *Construction of predictive features of lncRNAs associated with C2H2 zinc fingers*

Using the "limma" software, we examined the relationship between the CHZFs and lncRNAs. Data, including the expression data, of 1,157 CHZFLs were gathered and, the following screening parameters were employed: $|R^2| > 0.4$, and P<0.001. Univariate Cox regression modelling was used to identify the CHZFLs associated with the prognosis of ccRCC patients. CHZFLs were subsequently developed utilizing least absolute shrinkage and selection operator (LASSO) Cox regression analysis in order to generate prognostic features. We used LASSO regression for variable selection to simplify the model and a 10-fold cross-validation approach for internal validation with pi incidence as the dependent variable and Lambda. Min was selected as λ filter variable. The following formula was employed for this analysis: risk score = coef (lncRNA1) × expr (lncRNA1) + coef (lncRNA2) × expr (lncRNA2) + ... + coef (lncRNAn) × expr (lncRNAn), where "coef (lncRNAn)" denotes the coefficient associated with lncRNA survival, and "expr

 

**Table 1** Clinicopathologic characteristics of patients in different groups

| Variables | Entire TCGA dataset (n=507) | Internal validation cohort | |
|---|---|---|---|
| | | Training group (n=255) | Testing group (n=252) |
| Age (years), n (%) | | | |
| ≥65 | 336 (66.3) | 175 (68.6) | 161 (63.9) |
| <65 | 171 (33.7) | 80 (31.4) | 91 (36.1) |
| Gender, n (%) | | | |
| Female | 174 (34.3) | 95 (37.3) | 79 (31.3) |
| Male | 333 (65.7) | 160 (62.7) | 173 (68.7) |
| Grade, n (%) | | | |
| G1+2 | 227 (44.8) | 105 (41.2) | 122 (48.4) |
| G3+4 | 272 (53.6) | 145 (56.9) | 127 (50.4) |
| Unknown | 8 (1.6) | 5 (1.9) | 3 (1.2) |
| Stage, n (%) | | | |
| I + II | 306 (60.4) | 151 (59.2) | 155 (61.5) |
| III + IV | 198 (39.0) | 102 (40.0) | 96 (38.1) |
| TX + unknown | 3 (0.6) | 2 (0.8) | 1 (0.4) |
| T, n (%) | | | |
| T1+2 | 324 (63.9) | 162 (63.5) | 162 (64.3) |
| T3+4 | 183 (36.1) | 93 (36.5) | 90 (35.7) |
| M, n (%) | | | |
| M0 | 401 (79.1) | 200 (78.4) | 201 (79.8) |
| M1 | 78 (15.4) | 41 (16.1) | 37 (14.7) |
| MX + unknown | 28 (5.5) | 14 (5.5) | 14 (5.5) |
| N, n (%) | | | |
| N0 | 225 (44.4) | 114 (44.7) | 111 (44.0) |
| N1 | 16 (3.2) | 9 (3.5) | 7 (2.8) |
| NX | 266 (52.4) | 132 (51.8) | 134 (53.2) |

TCGA, The Cancer Genome Atlas; X, unable to evaluated; T, tumor; M, metastasis; N, lymph node.

(lncRNAn)" represents lncRNA expression.

Based on the median risk score, the ccRCC patients were divided into high- and low-risk groups. The survival rates of the two groups were compared using a Kaplan-Meier survival analysis. In PCA, "Limma" and "scatterplot3d" were utilized to illustrate the performance capabilities of various risk groups in cluster analysis (31,32). Univariate and multivariate Cox regression analyses were conducted to assess the relationship between risk scores and clinical factors. The accuracy and capabilities of the prediction signature were verified using the R timeROC package (33). To verify that the prediction signature was appropriate, all techniques were also incorporated into the internal validation cohort.

### *Construction of nomograms*

The risk score was merged with age, sex, grade, stage, and

 

clinicopathological features of the metastasis (M) stage to generate nomogram survival maps that could predict the 1-, 2-, 3-, and 5-year survival rates of the patients with renal cancer. The predicted survival rate was then compared to the actual survival rate, and calibration curves were used to determine consistency.

### *Drug sensitivity analysis with predictive signatures*

Using the Genomics of Drug Sensitivity in Cancer (GDSC) database, we investigated the role of various factors in predicting the response of patients to ccRCC treatment. Data on cancer cell drug sensitivity and molecular markers of therapeutic response were gathered from a public resource (34). The GDSC2 gene expression profiles and associated drug response data were retrieved using the oncoPredict tool (35). Sensitivity ratings were used to predict each medication's 50% maximum inhibitory concentration (IC50) value in ccRCC patients.

### *Immune infiltration analysis*

A single-sample gene set enrichment analysis (ssGSEA) was used to compare the immune cell populations and pathways among both groups. Using the ssGSEA, we assessed the penetration scores of 16 immune cell types, and the activity of 13 immunological-related pathways (36). Finally, differences in the levels of gene expression between the high- and low-risk groups were examined to investigate the relationship between the risk score and the immunologic checkpoints.

### *Statistical analysis*

All the statistical analyses were conducted using R software (version 4.2.1). The Wilcoxon test was used to compare the expression levels of the differentially expressed genes (DEGs) associated with the CHZFs in the normal and cancer tissues. The univariate and multivariate Cox models showed that the CHZFLs were independent predictive risk factors for ccRCC. The accuracy of the CHZFL model in predicting ccRCC was assessed using the area under the curve (AUC) of the receiver operating characteristic (ROC) curve. A P value of 0.05 was considered statistically significant for all two-sided statistical tests. The Bioconductor package (version 3.5.5) and the R environment were used for the statistical analysis.

## Results

### *Enrichment analysis of differently expressed genes related to zinc finger type C2H2*

Using the procedure shown in *Figure 1*, 103 C2H2 zinc finger-related DEGs were identified, of which 61 were upregulated and 42 were downregulated (*Figure 2A*; available online: https://cdn.amegroups.cn/static/public/tau-2024-769-2.xls). The GO and KEGG-based enrichment analyses showed that the C2H2 zinc finger-associated DEGs were enriched in three primary pathways; that is, signaling pathways linked with herpes simplex virus type 1 infection; chronic myeloid leukemia; and transcriptional dysregulation in cancer (*Figure 2B*). The GO analysis revealed that the primary areas of enrichment for the biological process category of the DEGs were leukocyte differentiation regulation, glycogenesis and regulation, and hematopoietic regulation processes; those for the cellular component category were transcriptional regulatory complexes; and those for the molecular function category were DNA-binding transcriptional repressor activity and DNA-binding transcriptional activator activity (*Figure 2C*).

### *Construction of a predictive model*

We screened 1,157 lncRNAs associated with differentially expressed C2H2-type ZFPs (available online: https://cdn.amegroups.cn/static/public/tau-2024-769-3.xls). The univariate Cox regression analysis showed that 235 lncRNAs were associated with the prognosis of ccRCC patients. Prognostic models of the prognosis-related lncRNAs were established, and 1,000 cross-validation runs were performed to predict the prognosis of patients with ccRCC (*Figure 3A,3B*). The prediction model contained the following five genes: DBH-AS1, LINC02100, AC026401.3, AC124854.1, and AL117336.2, which have been associated to C2H2 type zinc fingers. The expression levels of the five CHZFLs in the ccRCC patients were examined (*Figure 3C*). Two R software programs, ggalluvial and cytoscape, were utilized to visualize additional model genes. The results for 26 pairs of lncRNA-mRNAs were obtained using a co-expression network (*Figure 3D*). ZNF189 and ZNF395 were expressed together with AC124854.1; AC026401.3 was expressed together with ZNF692; LINC02100 was expressed together with IKZF1, IKZF3; ZNF26, ZNF121, GFI1, and BCL11B, DBH-AS1 were co-expressed with

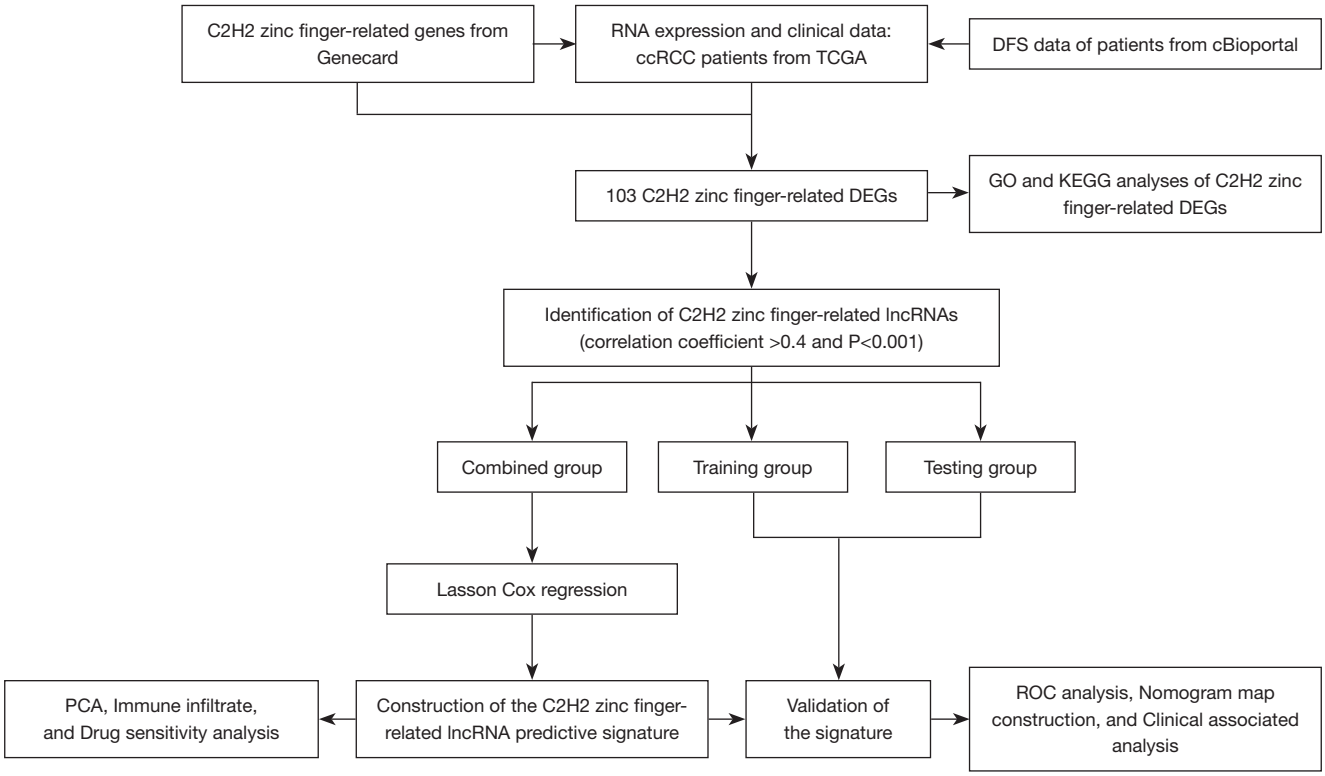


**Figure 1** Study flow chart. C2H2, Cys2His2; ccRCC, clear cell renal cell carcinoma; TCGA, Cancer Genome Atlas; DFS, disease-free survival; DEGs, differentially expressed genes; GO, Gene Ontology; KEGG, Kyoto Encyclopedia of Genes and Genomes; lncRNAs, long non-coding RNAs; PCA, principle component analysis; ROC, receiver operating characteristic.

ZNF276, ZNF83, ZNF692, ANKZF1, GFI1, ZNF767P, and ZNF337; and AL117336.2 was co-expressed with ZNF44, ZNF276, ZMAT1, ZNF83, ZNF26, ZNF121, ZNF767P, ZNF354B, ZNF337, and ZNF841. AL117336.2, AC026401.3, DBH-AS1, and LINC02100 were risk factors, while AC124854.1 was a protective factor (*Figure 3E*). The following formula was established: risk score = 0.654 × AL117336.2 expression + 0.315 × AC026401.3 expression – 0.380 × AC124854.1 expression + 0.269 × DBH-AS1 expression + 0.256 × LINC02100 expression.

### *Analysis of the relationship between outcomes and prognostic factors in ccRCC patients*

The risk-score formula was used to calculate every patient's risk score, and the patients were then divided into high- and low-risk groups according to the median value. A Kaplan-Meier analysis was used to assess the OS times of the two groups. The findings showed that the OS time of the low-risk group was substantially longer than that of the high-risk the group (*Figure 4A*). The risk rating difference is shown in *Figure 4B*, and it is evident that more deaths occurred as the probability score increased (*Figure 4C*).

In the univariate Cox regression analysis results, the OS of the ccRCC patients was strongly associated with age, grade, stage, tumor (T) stage, and risk score (*Figure 4D*). Additionally, age, grade, and risk score were independently predictors of OS in the multivariate Cox regression analysis. These findings were then used to determine whether the risk features were independent variables that affected the future survival of ccRCC patients (*Figure 4E*).

Other clinicopathological indicators had a lower predictive value than the AUC of the risk score (AUC =0.775) (*Figure 4F*). These 1-, 3-, and 5-year survival AUCs demonstrated strong predictive accuracy. As *Figure 4G* shows, the AUC was divided into 0.742, 0.727, and 0.783. To examine the impact of these variables, the clinicopathological features of the groups were compared with the greatest risk. However, no significant differences between the high-risk and low-risk groups were found

 

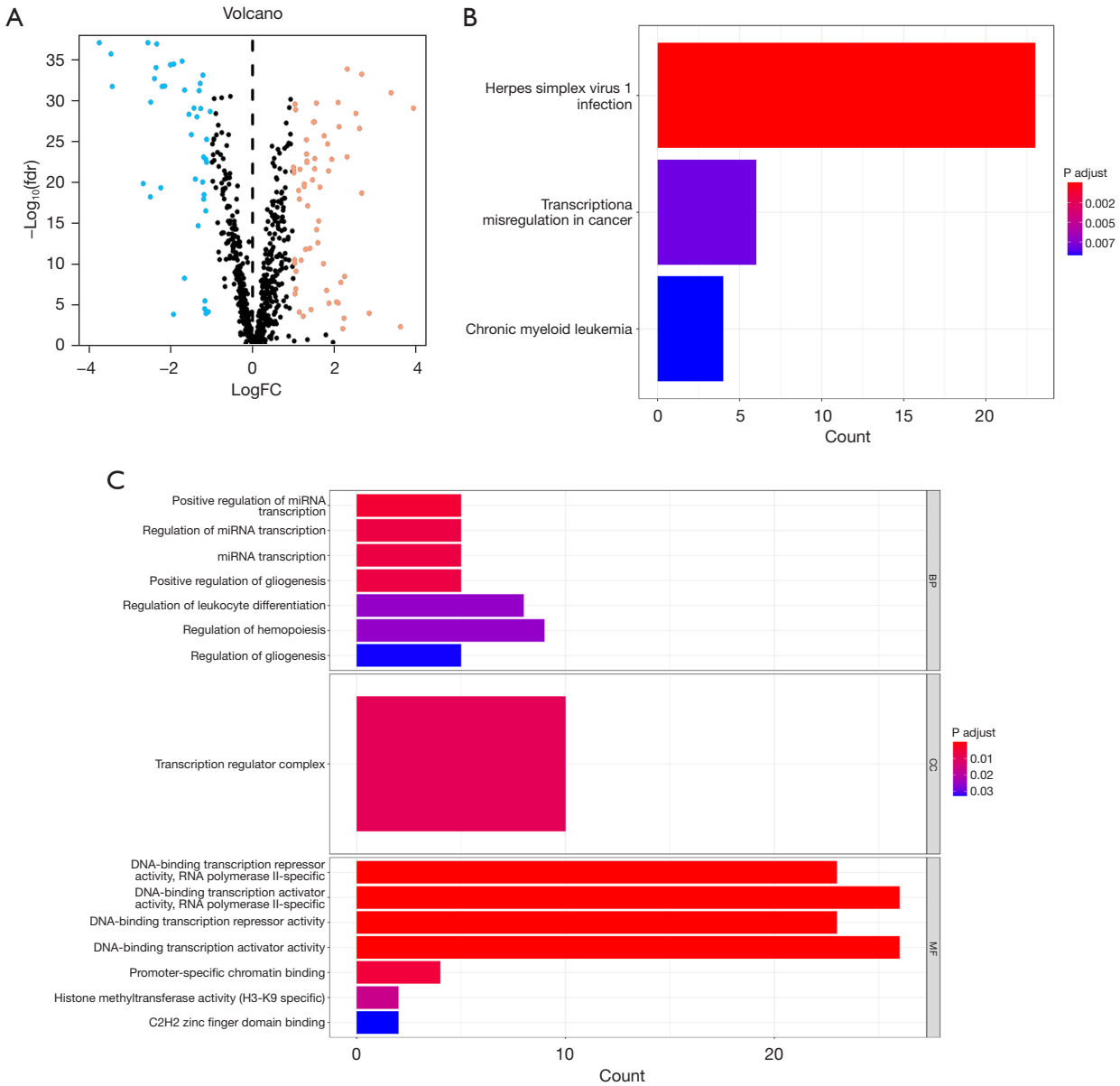


**Figure 2** GO and KEGG analyses of C2H2 zinc finger-related DEGs in cancer and adjacent tissues. (A) 103 genes in the ccRCC are linked to the C2H2 zinc fingers. Genes that are up-regulated are denoted by orange dots, and those that are down-regulated are denoted by blue dots. The black dots represent genes whose expression is neither up-regulated nor down-regulated. (B) KEGG analysis of DEGs connected to C2H2 zinc fingers. (C) GO analysis of DEGs connected to the C2H2 zinc finger. FC, fold change; FDR, false discovery rate; C2H2, Cys2His2; BP, biological process; CC, cellular composition; MF, molecular function; GO, Gene Ontology; KEGG, Kyoto Encyclopedia of Genes and Genomes; DEGs, differentially expressed genes.

(*Figure 5*).

To further predict the prognosis of ccRCC patients, we created nomogram predicting models that combined both clinicopathological variables and risk ratings to predict 1-, 3-, and 5-year survival (*Figure 6A*). The actual OS and the anticipated survival rates were consistent after calibration (*Figure 6B-6D*).

***Association between prediction variables and other***

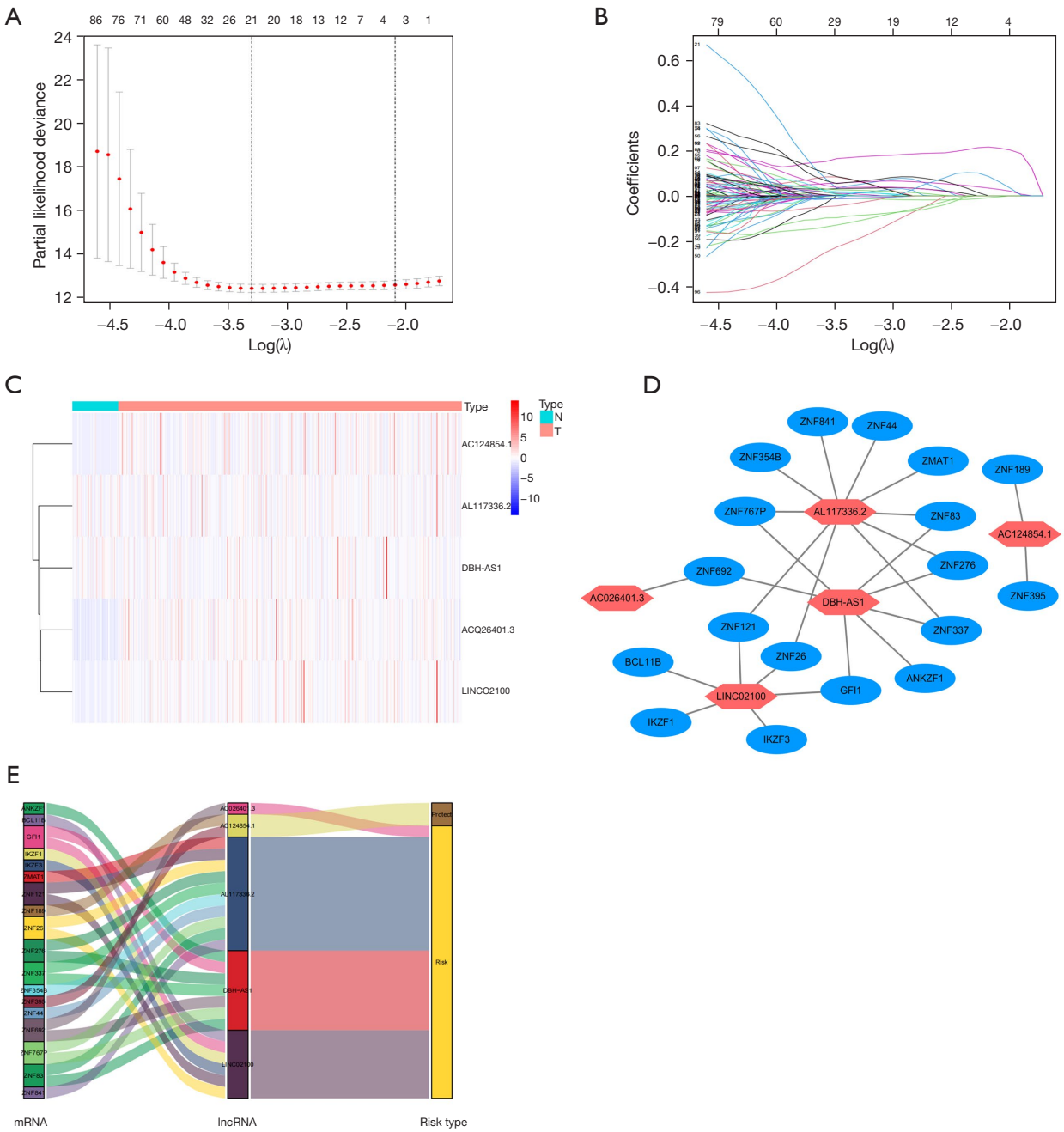


**Figure 3** Establishment of a predictive lncRNA signature and a lncRNA-mRNA network of five lncRNAs related to C2H2 zinc fingers. Tuning parameters with 10-fold cross-validation. (A) 10-fold cross-validation error rate plots. (B) LASSO coefficient profiles of five C2H2 zinc finger-associated lncRNAs. The levels of expression and a lncRNA-mRNA network of five lncRNAs related to the C2H2 zinc finger in the predictive signature. (C) Expression levels of five C2H2 zinc finger-associated lncRNAs in ccRCC and normal tissues. (D) Co-expression networks of prognostic C2H2 zinc finger-associated lncRNAs. (E) Mulberry plot of prognostic C2H2 zinc finger-associated lncRNAs. mRNA, messenger RNA; lncRNAs, long non-coding RNAs; C2H2, Cys2His2; LASSO, least absolute shrinkage and selection operator; ccRCC, clear cell renal cell carcinoma.

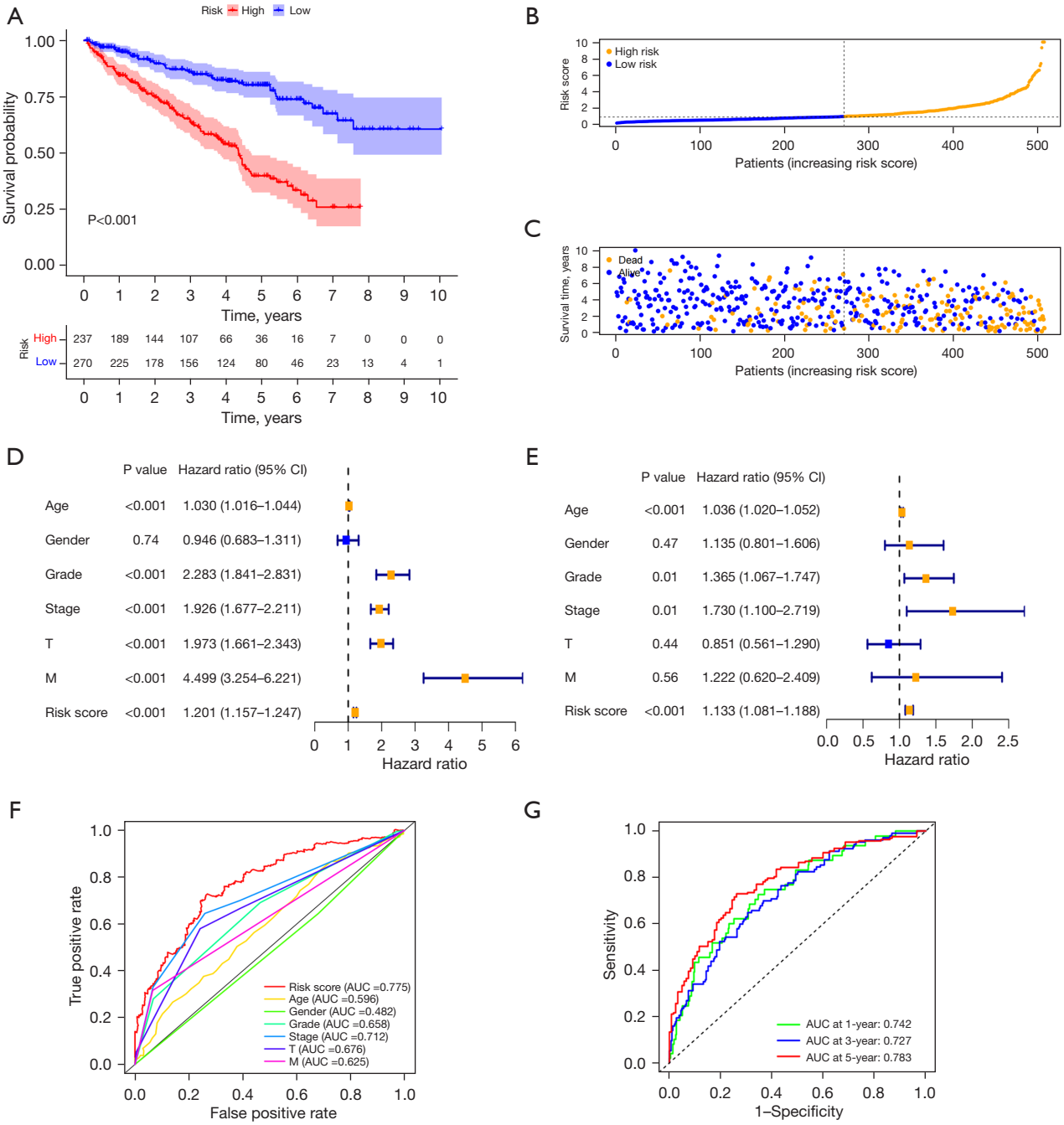


**Figure 4** Association between prognosis and prognostic characteristics in patients with ccRCC. (A) Kaplan-Meier survival analysis of high- and low-risk ccRCC patients. (B) The distribution of risk scores among patients with ccRCC. (C) The number of fatalities and survivors with various risk scores. A blue blot indicates the number of survivors, and a yellow blot indicates the number of fatalities. (D) The univariate Cox regression analysis forest plot. (E) The multivariate Cox regression analysis forest plot. (F) ROC curve of the risk score and clinicopathological factors. (G) ROC curve and AUCs of 1-, 3-, and 5-year survival rates. T, tumor; M, metastasis; AUC, area under the curve; ccRCC, clear cell renal cell carcinoma; ROC, receiver operating characteristic.

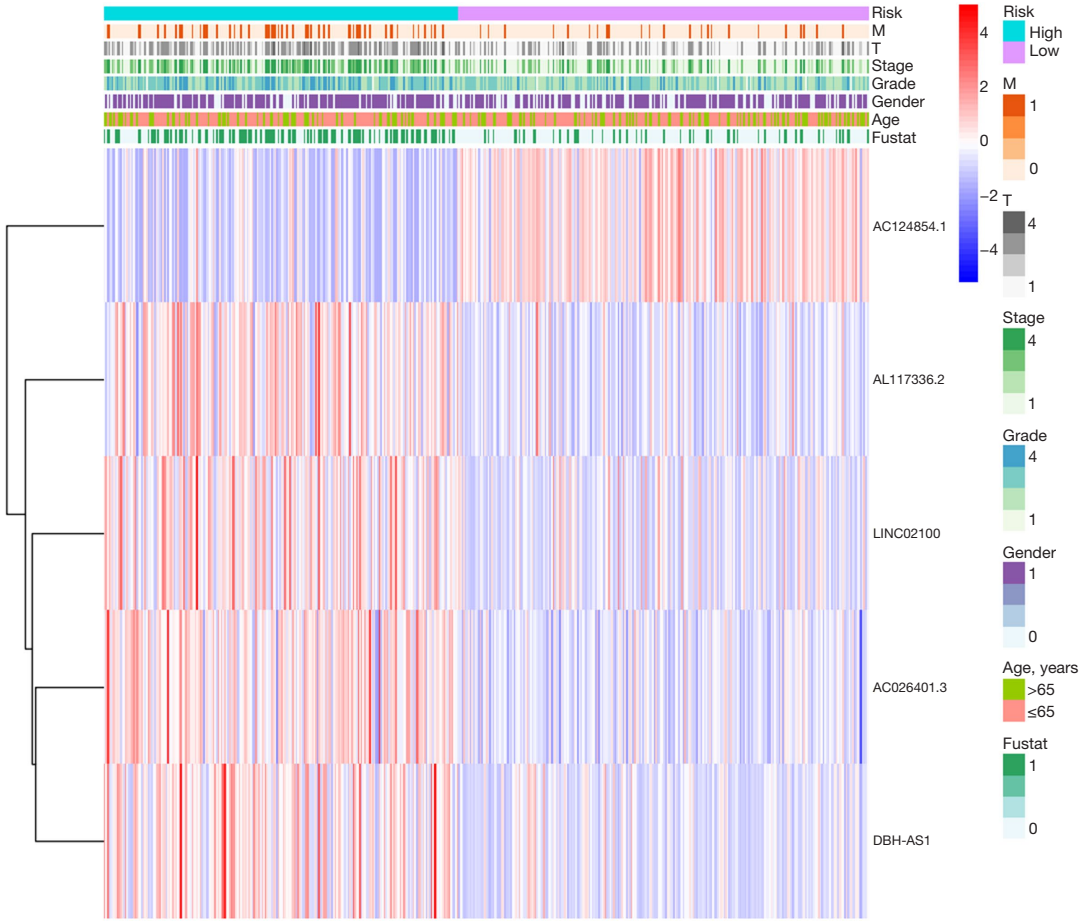


**Figure 5** Heat map of prognosis-related lncRNAs and clinicopathological factors in high- and low-risk groups. M, metastasis; T, tumor; lncRNAs, long non-coding RNAs.

### *clinicopathologic markers in ccRCC patients*

To examine the relationship between prognosis and predictive characteristics in patients with ccRCC, who were categorized by various clinicopathological factors, a subgroup analysis of survival was performed in patients with different ages, pathological types, grades, and T, M, and node (N) stages. The results showed that OS was substantially lower in the high-risk group than the low-risk group (*Figure* 7). These findings show that, even when several clinicopathological factors are present, predictive characteristics may foresee the outcome of patients with ccRCC.

### *Verification of predictive features internally*

We divided the ccRCC patients into two groups at random to confirm the validity of the prognostic prediction signature based on the complete TCGA dataset. *Table 1* displays the demographics of the two patient groups. In line with the findings for the whole dataset, the high-risk group performed worse than the low-risk group in the training group (*Figure 8A*, P=4.09e−08). In the validation group, the OS percentage of the high-risk group was lower than that of the low-risk group (*Figure 8B*, P=1.05e−06). We examined the patients' clinical presentations and the ROC curves of the two groups. The AUCs of the 1-, 3-, and 5-year survival

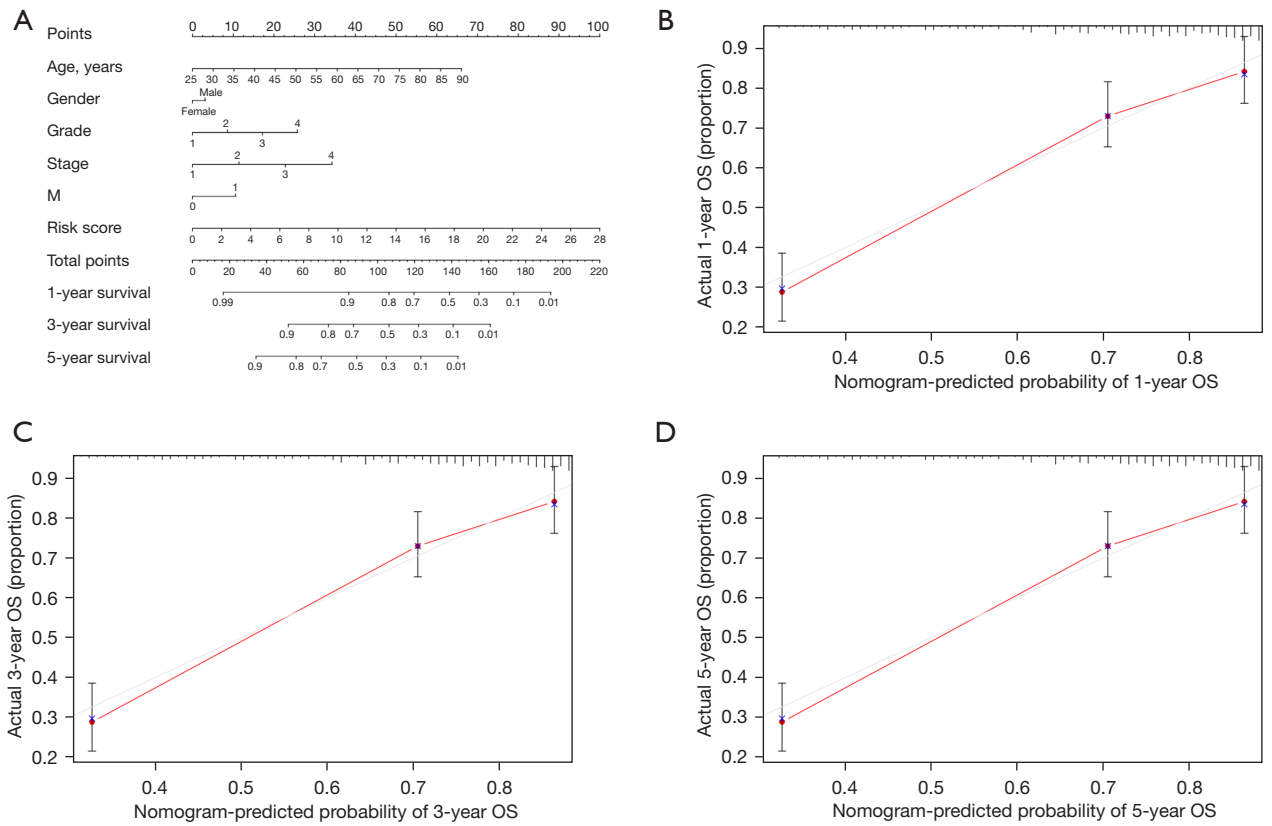


**Figure 6** Development and validation of a nomogram. (A) Nomogram predicting 1-, 3-, and 5-year survival in ccRCC patients. (B-D) The calibration curve examines the agreement between the 1-, 3-, and 5-year predicted survival rates and the actual OS rates. M, metastasis; OS, overall survival; ccRCC, clear cell renal cell carcinoma.

rates for the training group were 0.740, 0.735, and 0.812, respectively (*Figure 8C*). The AUCs of the 1-, 3-, and 5-year survival rates for the validation group were 0.751, 0.728, and 0.764, respectively (*Figure 8D*).

### *Immune cell infiltration and functional analysis*

To visualize the spatial distribution of the high- and low-risk groups, a PCA was conducted to examine the patient distribution based on genome-wide, C2H2 zinc finger-related gene sets, C2H2 zinc finger-related lncRNAs, and predictive features. Patients were allocated to high- and low-risk groups based on the predictive factors (*Figure 9*). To investigate the connection between risk scores, immunity, and function in patients with ccRCC, we used ssGSEA to measure the activity levels of immune cell subsets and the functions that go along with them. The results showed that there were significant differences between the high- and low-risk groups in terms of T helper cells, T follicular helper cells, T helper type 1 cells, T helper type 2 cells, macrophages, mast cells, triggered dendritic cells, (CD)8-positive (+) T cells, immature dendritic cells, and tumor-infiltrating lymphocytes (TILs) (*Figure 10A*). The immunological functions of chemokine receptors, checkpoints, cytolytic activity, inflammatory promotion, para-inflammation, T cell co-inhibition, T cellular co-stimulation, and the type I interferon (IFN) response were all found to be more highly scored in the high-risk group than the low-risk group (*Figure 10B*). Further, immune checkpoint expression was also found to differ between the two groups (*Figure 10C*).

### *Correlation analysis of predictive signature with ccRCC treatment*

Drug sensitivity scores were predicted using the OncoPredict program for both the high- and low-risk groups, and a strong correlation with chemotherapeutic

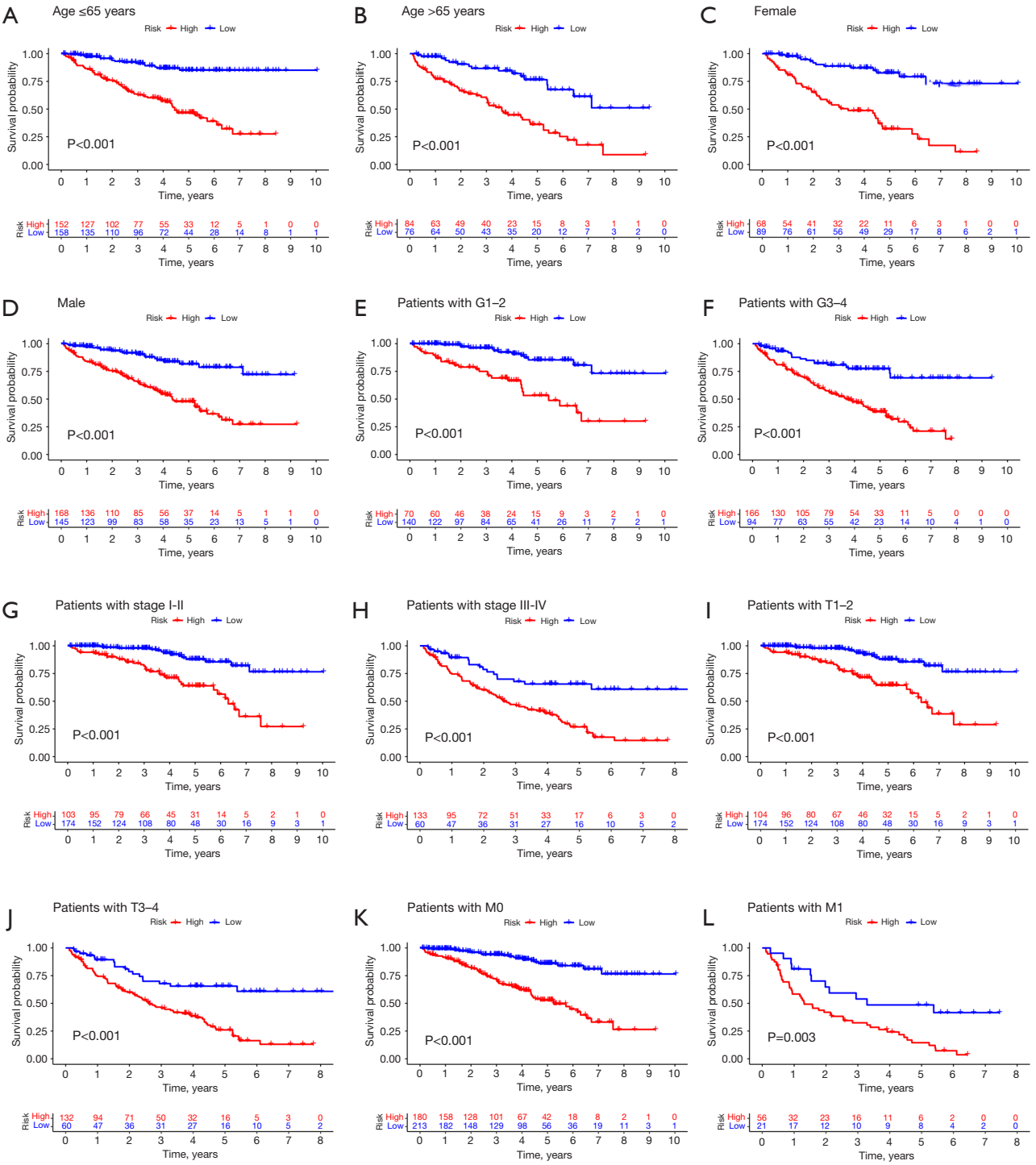


**Figure 7** Kaplan-Meier survival curves of high- and low-risk patients ranked by clinicopathological characteristics. (A,B) Age. (C,D) Gender. (E,F) Grade. (G,H) Stage. (I,J) T stage. (K,L) M stage. T, tumor; M, metastasis.

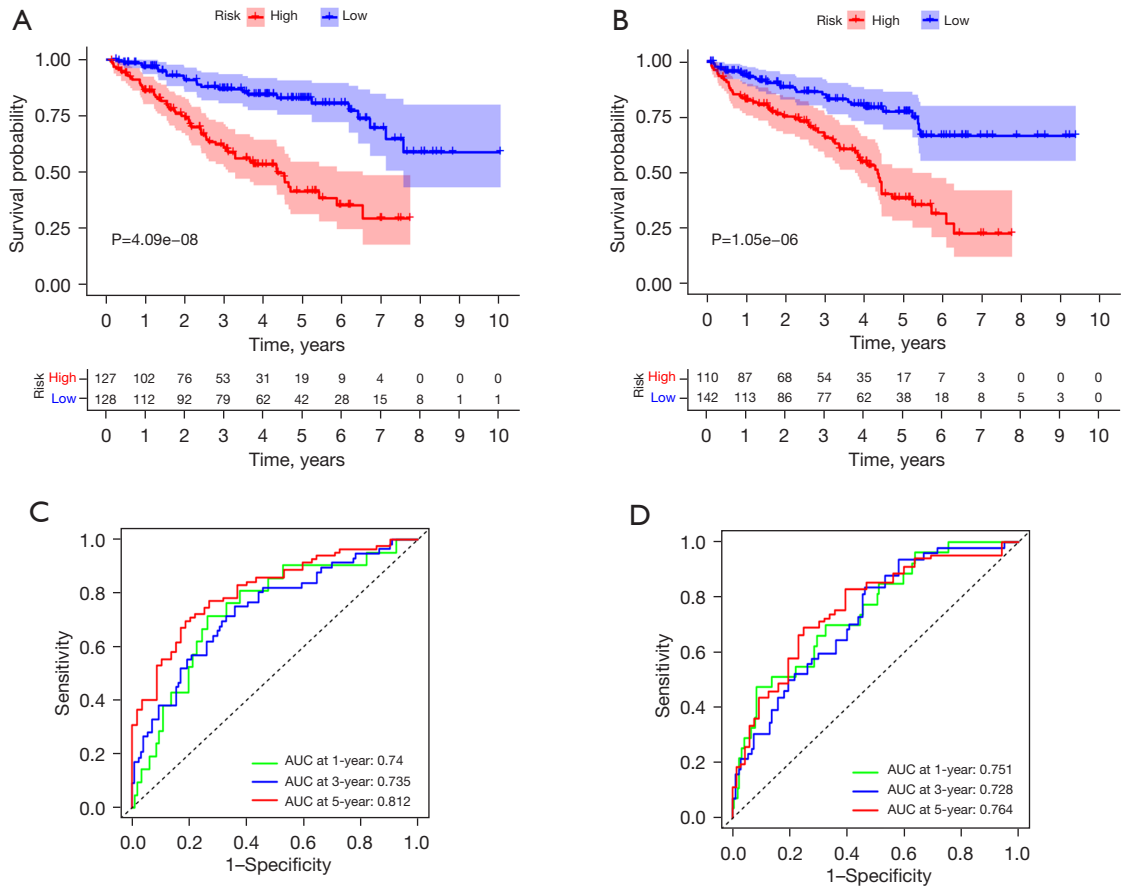


**Figure 8** Validation of OS prediction signatures on the internal platform based on different datasets. (A) Kaplan-Meier survival curves of the training group. (B) Kaplan-Meier survival curves of the testing group. (C) 1-, 3-, and 5-year ROC curves and AUCs for the training group. (D) 1-, 3-, and 5-year ROC curves and AUCs for the testing group. AUC, area under the curve; OS, overall survival; ROC, receiver operating characteristic.

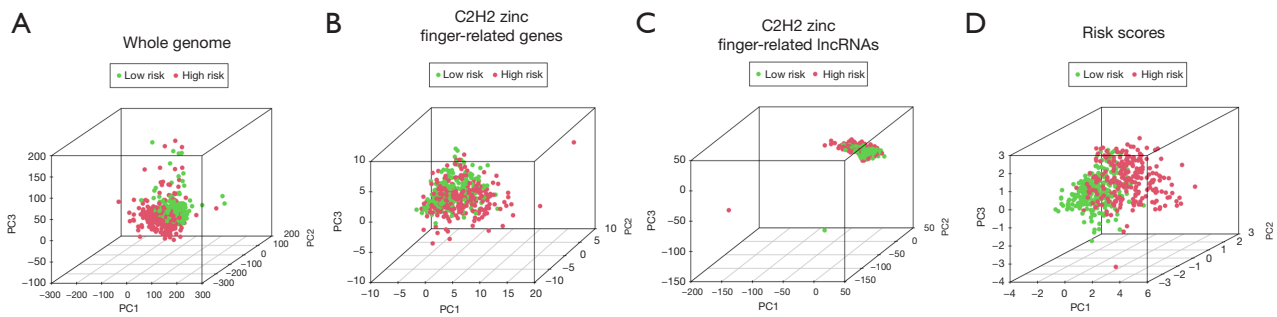


**Figure 9** PCA profiles showed patient distribution based on (A) genome-wide; (B) C2H2 zinc finger-related genes; (C) C2H2 zinc finger-related lncRNAs; and (D) risk scores. Red and green dots were more clearly separated in the high- and low-risk groups, respectively. C2H2, Cys2His2; lncRNAs, long non-coding RNAs; PCA, principle component analysis.

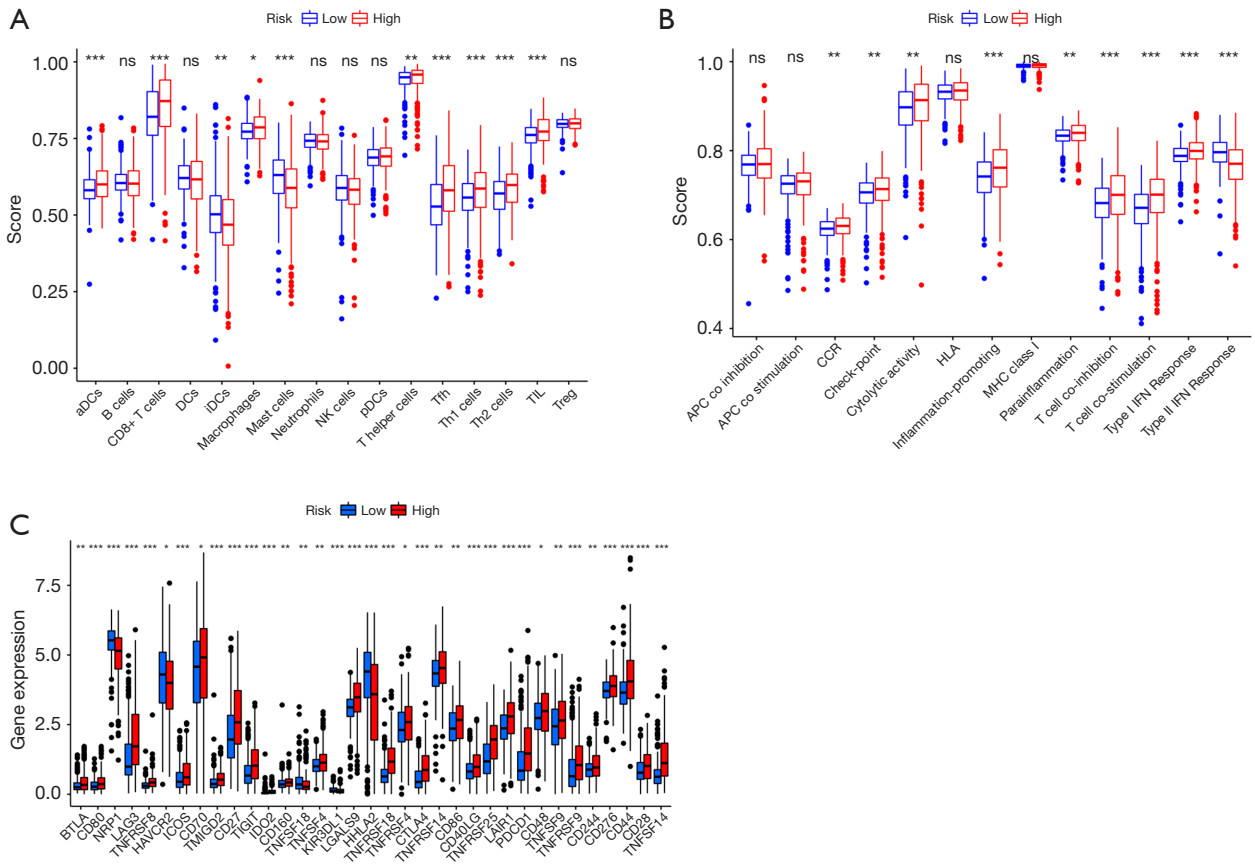


**Figure 10** Immune infiltration analysis: ssGSEA score results. (A) 16 immune cell scores. (B) 13 immune-related function scores. (C) Expression of immunological checkpoints in high- and low-risk groups. ns, no significance; *, P<0.05; **, P<0.01; ***, P<0.0001. aDCs, activated dendritic cells; DCs, dendritic cells; iDCs, immature dendritic cell; NK, natural killer; pDC, plasmacytoid dendritic cells; Tfh, follicular helper T cells; TIL, tumor-infiltrating lymphocyte; Treg, regulatory T cells; APC, antigen presenting cells; CCR, CC chemokine receptor; HLA, human leukocyte antigen; MHC, major histocompatibility complex; IFN, interferon; ssGSEA, single-sample gene set enrichment analysis.

drug IC50 values was found. The high-risk group had heightened sensitivity to cytarabine, epirubicin, gemcitabine, and vinorelbine (*Figure 11A-11D*). The low-risk group had heightened susceptibility to dihydrorotenone, P22077, CDK1 inhibitor RO3306, and TGF-R inhibitor SB505124 (*Figure 11E-11H*). Further investigations should be conducted to determine which individual chemotherapy regimens are appropriate for patients classified as high and low risk.

### *Development of anticipated DFS characteristics for zinc finger-associated lncRNAs of the C2H2 type*

Additionally, to account for the predictive value of DFS in patients with ccRCC, we established a DFS prediction lncRNA signature linked to C2H2 zinc fingers. We retrieved DFS data from the cBioPortal database for 111 ccRCC patients. The univariate Cox regression analysis showed that 43 CHZFLs were substantially linked with DFS in ccRCC patients. We used multivariate Cox regression analysis for developing prediction models. The risk score was calculated as follows: risk score = −2.176 × AL031186.1 − 3.441 × JPX. Based on the median risk score, the patients were divided into two high- and low-risk groups. The Kaplan-Meier survival curve analysis revealed that the DFS time of the high-risk group was significantly shorter than that of the low-risk group (*Figure 12A-12C*, P<0.001). The AUCs of the 1-, 3-, and 5-year survival rates were 0.761, 0.754, and 0.795, respectively (*Figure 12D*).

To determine whether predictive characteristics might

 

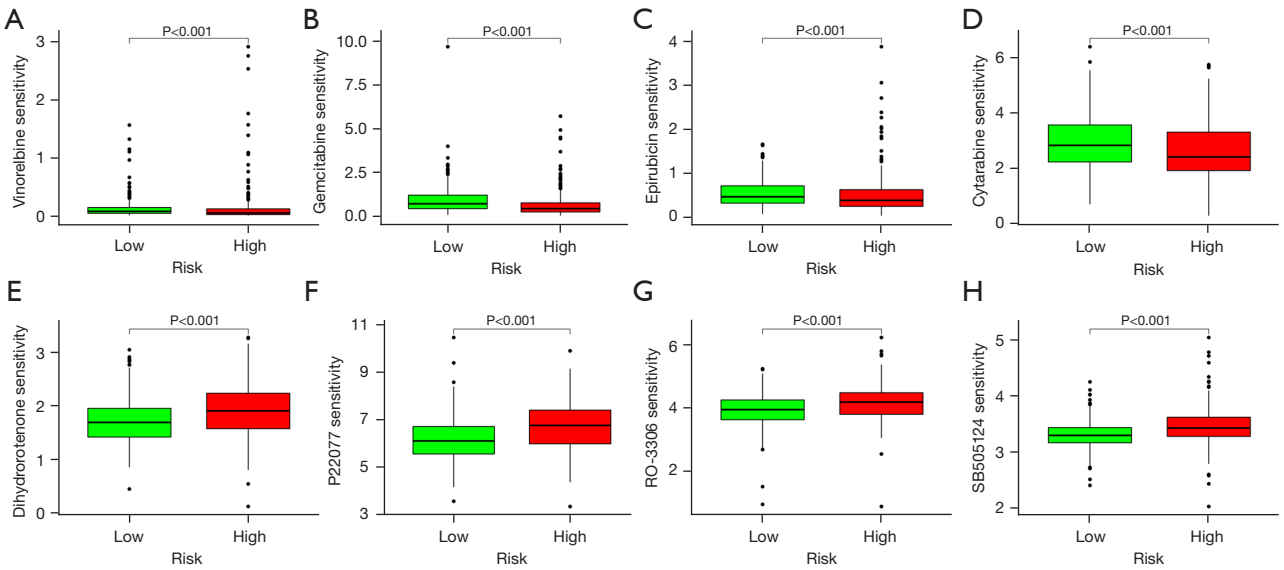


**Figure 11** Drug sensitivity analysis. (A-D) Vinorelbine, gemcitabine, epirubicin, and cytarabine are candidates for chemotherapy in patients with high CHZFLs scores. (E-H) Dihydrorotenone, P22077, RO-3306, and SB505124 are candidates for chemotherapy in patients with low CHZFLs scores. CHZFLs, Cys2His2 zinc finger-associated long non-coding RNAs.

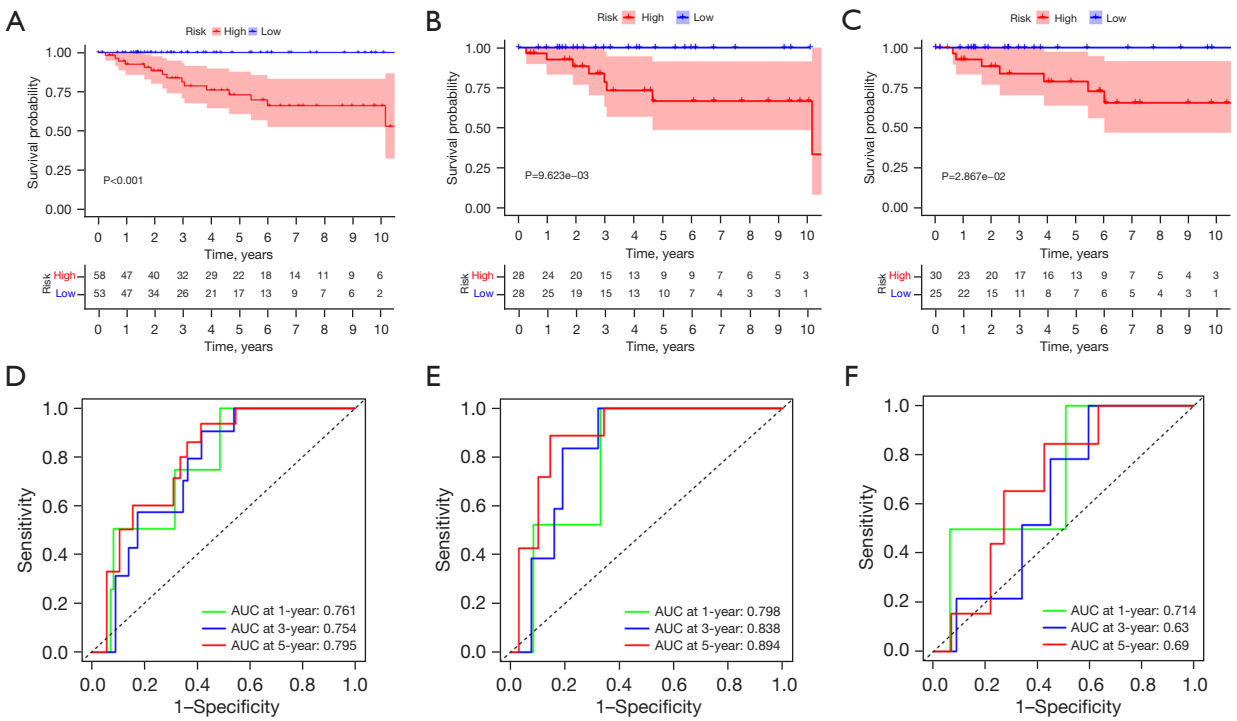


**Figure 12** The predictive value of C2H2 zinc finger-associated lncRNA signaling for DFS is being evaluated. (A) Kaplan-Meier survival curves for the whole dataset. (B) Kaplan-Meier survival curves for the first group of patients. (C) Kaplan-Meier survival curves for the second group of patients. (D) ROC curves and AUCs for the 1-, 3-, and 5-year survival rates for the whole dataset. (E) ROC curves and AUCs for the 1-, 3-, and 5-year survival rates for the first group of patients. (F) ROC curves and AUCs for the 1-, 3-, and 5-year survival rates for the second group of patients. AUC, area under the curve; C2H2, Cys2His2; lncRNA, long non-coding RNA; DFS, disease-free survival; ROC, receiver operating characteristic.

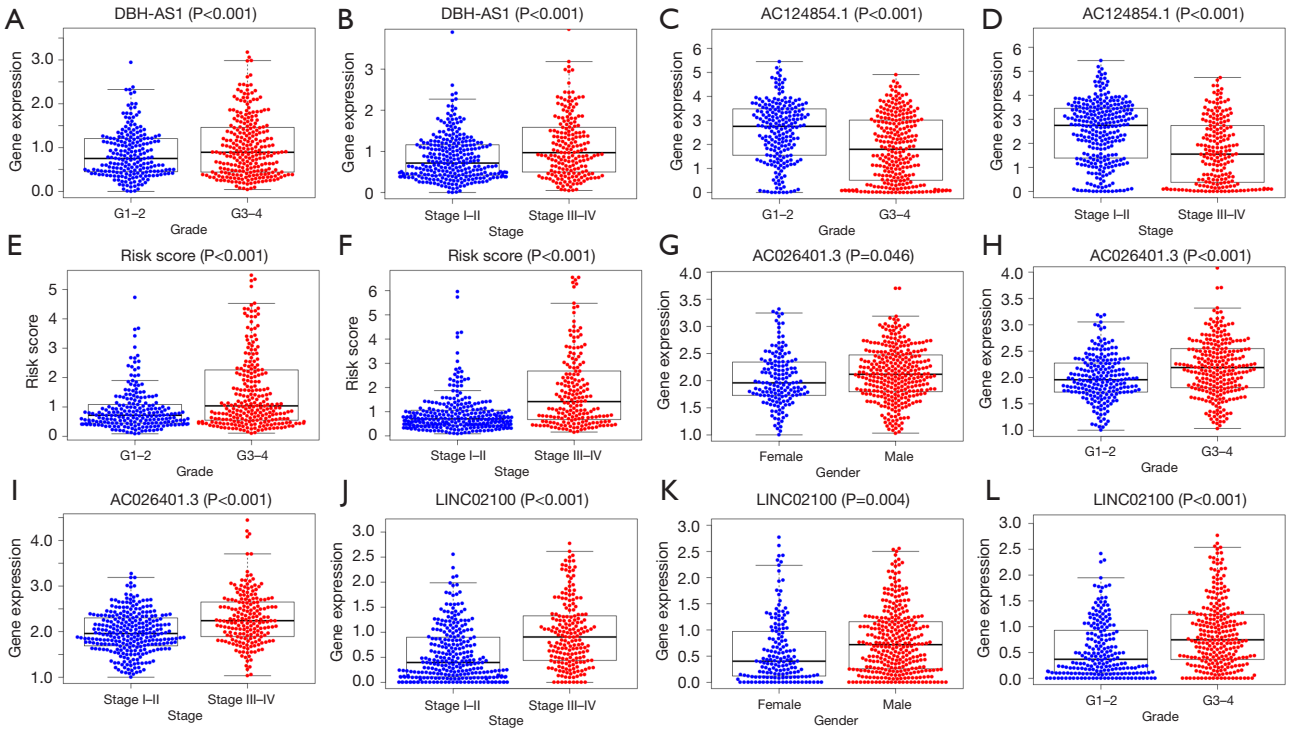


**Figure 13** A correlation analysis was performed between the CHZFLs and clinical features. (A,B) Relationship between DBH-AS1 expression level, and grade and stage. (C,D) Relationship between AC124854.1 expression level, and stage, and grade. (E,F) Relationship between risk score, and grade, and stage. (G-I) Relationship between AC026401.3 expression level, and sex, tumor grade, and stage. (J-L) Relationship between LINC02100 expression level, and sex, tumor grade, and stage. CHZFLs, Cys2His2 zinc finger-associated long non-coding RNAs.

be applied to DFS, 11 patients were divided into the first and second internal cohorts at random (n=56 and n=55, respectively). After the complete dataset was analyzed, the patients were categorized into low- and high-risk groups based on the median. Patients in a high-risk group had a shorter DFS time in the first internal cohort (*Figure 12B*, P=9.623e–03) and the second internal cohort (*Figure 12C*, P=2.867e–02) than those in the low-risk group. The AUCs of the 1-, 3-, and 5-year survival rates for the first internal cohort were 0.798, 0.838, and 0.894, respectively (*Figure 12E*). While the AUCs of the 1-, 3-, and 5-year survival rates in the second internal cohort were 0.714, 0.630, and 0.690, respectively (*Figure 12F*).

### *Relationship between clinical factors and risk scores/ CHZFLs*

Using the gene expression and related clinical data we gathered from TCGA database, we examined the connection between the clinical parameters and the risk scores of the five CHZFLs. The findings demonstrated that the expression levels of AC026401.3 and LINC02100 were correlated with gender, tumor stage, and tumor grade; the expression levels of DBH-AS1, AC124854.1, and risk score were correlated with tumor stage and grade (*Figure 13*).

## Discussion

The pathophysiology of KIRC, a disease of the renal parenchyma's urothelial system, is highly complex. In most cases, KIRC is resistant to radiotherapy and chemotherapy; hence, surgery is the mainstay of treatment. It is estimated that 30% of cancer patients may experience metastases even with early surgical intervention (37). More biomarkers will be discovered as bioinformatics technology advances, and some of these biomarkers may someday be used as targets for ccRCC diagnosis and treatment. Specialized markers can increase the accuracy of predictions (38,39); however, the heterogeneity of the ccRCC prevents us from meeting our requirements for outcome prediction by a single molecular

marker. The other side of the coin is monitoring the response of current immunotherapy based not only on imaging studies, but also personalized biomarkers yet to be established. The creation of multivariate models to foresee cancer prognosis is currently a popular area of research, then.

Numerous studies have shown the importance of the C2H2 ZFP in the development of malignant tumours. ZNF692 activates the MEK/ERK pathway via TNK2 to increase osteosarcoma cell motility, invasion, and proliferation (40). The C2H2 zinc finger family member ZNF384 can cause DNA double-strand breaks, which aid in the growth of cancer (41). ZNF471 inactivates PI3K/AKT/mTOR signaling in conjunction with BANP to reduce tumor malignancy; however, it is frequently inhibited by aberrant promoter methylation in RCC (22). In cholangiocarcinoma, the RBM10 C761Y mutation was shown to control β-catenin signaling and produce carcinogenic abnormal spindle microtubule assembly (ASPM) isoforms (42). The differential expression of C2H2 ZFPs in RCC and its possible predictive significance are of great interest, as they play a role in the occurrence, development, and progression of cancers. The advancement of tumor immunology has allowed for a greater understanding of malignancies (43). Tumor cells evade immune control in various ways, causing them to proliferate quickly inside the body, which is called "immune escape" (44). The host immune system may become more aggressive against tumor cells due to immune checkpoint blockade therapy based on PD-1/PD-L1 (45,46). Drug resistance is currently the biggest problem facing the treatment of ccRCC (47). Additionally, there has been an increase in interest in the function of lncRNAs in cancer (48,49).

Via the implementation of univariate Cox and LASSO regression analyses, we were able to identify the CHZFLs linked to prognosis, including AL117336.2, AC026401.3, AC124854.1, DBH-AS1, and LINC02100. To investigate whether the CHZFLs could serve as prognostic factors, we developed a unique prognostic prediction technique based on each of these five genes. To the best of our knowledge, this model is the first prediction risk model of CHZFLs in RCC scenario. Both the univariate and multivariate Cox regression analyses showed that the risk model was a valid prognostic predictor for ccRCC. Survival and ROC analysis further showed the biological significance of this feature in predicting the prognosis of ccRCC patients compared to the model of Liu *et al.* (50). Nomogram analysis revealed an analogous situation, with risk indicators almost predicting OS in ccRCC patients. These markers are more accurate than other clinicopathological criteria in predicting outcomes, and our findings might be useful in choosing between immunotherapy and systemic treatment.

The clinical outcome of RCC is highly correlated with immune infiltration. According to the latest theory, the quantity and distribution of invasive immune cells play a crucial role in the development of cancer, the effectiveness of immunotherapy, and patient prognosis (citation missing). Tumor-infiltrating immune cells build a miniature ecosystem in the tumor microenvironment and may have prognostic value (51). Our ssGSEA results showed that activated dendritic cells, $CD8^+$ T cells, macrophages, T helper cells, and TILs were also involved in the development of the tumor microenvironment, and these cells had higher scores in the high-risk group. These findings not only support the important role of TILs in the tumor immune microenvironment, but also provide new perspectives for our understanding of the interaction between tumors and the immune system. Research has shown that dendritic cells, which are critical adaptive immune response regulators, are crucial in T-cell-mediated cancer immunity (52). A poor prognostic feature for head and neck squamous cell carcinoma is the immunological microenvironment with a high density of PD-1 + helper T cells in tumor cell nests (53). Patients with bladder cancer (BC) with high $CD8^+$ T-cell infiltration have a poor prognosis (54,55). The high infiltration of tumor-associated macrophages in advanced thyroid cancer has been linked to a poor prognosis (56). In addition to higher cancer immune cell infiltration, the high-risk group also had lower anti-tumor immunity and higher type I IFN response scores. Consequently, decreased antitumor immunity may contribute to a poor outcome in high-risk patients (citation missing).

Patients with advanced malignancies have a higher chance of survival when receiving immunotherapy based on checkpoint inhibitors (57). Between the high- and low-risk groups, immune checkpoint expression varied considerably, indicating variations in the sensitivity of immunotherapy. Our study also showed the high-risk patients had heightened sensitivity to traditional chemotherapeutic agents such as cytarabine, epirubicin, gemcitabine, and vinorelbine, which suggests that combining immunotherapy and chemotherapy can benefit high-risk patients. Thus, our findings provide us with a new idea that combined immunotherapy and chemotherapy may benefit high-risk RCC patients. This study had a number of limitations. First, we only used data from the TCGA database for the internal validation; future external validation with independent datasets will

 

provide a prospective perspective. Second, this study used retrospective data, leveraging information from open databases. Therefore, more prospective real-world data are needed to validate the clinical value of the TCGA database. Further, no *in vivo* and *in vitro* tests were conducted in this study. Future research should focus on the verification of the functionality of CHZFLs in ccRCC.

## Conclusions

This study created a CHZFL signature and validated the findings using various datasets to determine the prognosis of ccRCC patients. Additionally, CHZFLs were proved to be independent risk factors of ccRCC. Here, we proposed a novel tool to be used as an adjunct in the establishment of ccRCC prognosis. Diversifying accurately low- and high-risk cohorts, it can be easily incorporated for the patient's qualification for clinical trials.

## Acknowledgments

None.

## Footnote

*Reporting Checklist:* The authors have completed the TRIPOD reporting checklist. Available at https://tau.amegroups.com/article/view/10.21037/tau-2024-769/rc

*Peer Review File:* Available at https://tau.amegroups.com/article/view/10.21037/tau-2024-769/prf

*Funding:* This work was supported by the Natural Science Foundation of Jiangsu Province (Nos. BE2017682, MS2024032 and MS22022085) and the Basic Research and Social Minsheng Plan Project (Nos. JC22022021 and JC12022008).

*Conflicts of Interest:* All authors have completed the ICMJE uniform disclosure form (available at https://tau.amegroups.com/article/view/10.21037/tau-2024-769/coif). The authors have no conflicts of interest to declare.

*Ethical Statement:* The authors are accountable for all aspects of the work in ensuring that questions related to the accuracy or integrity of any part of the work are appropriately investigated and resolved. The study was conducted in accordance with the Declaration of Helsinki (as revised in 2013).



## References

1. Miller KD, Nogueira L, Mariotto AB, et al. Cancer treatment and survivorship statistics, 2019. CA Cancer J Clin 2019;69:363-85.
2. Chen YB. Update on Selected High-grade Renal Cell Carcinomas of the Kidney: FH-deficient, ALK-rearranged, and Medullary Carcinomas. Adv Anat Pathol 2024;31:118-25.
3. Shen C, Chen Z, Zhang Y, et al. Biochemical and clinical effects of RPS20 expression in renal clear cell carcinoma. Oncol Rep 2023;49:22.
4. Fernández-Pello S, Hofmann F, Tahbaz R, et al. A Systematic Review and Meta-analysis Comparing the Effectiveness and Adverse Effects of Different Systemic Treatments for Non-clear Cell Renal Cell Carcinoma. Eur Urol 2017;71:426-36.
5. Garcia JA, Rini BI. Recent progress in the management of advanced renal cell carcinoma. CA Cancer J Clin 2007;57:112-25.
6. Barata PC, Rini BI. Treatment of renal cell carcinoma: Current status and future directions. CA Cancer J Clin 2017;67:507-24.
7. Siegel RL, Miller KD, Jemal A. Cancer statistics, 2018. CA Cancer J Clin 2018;68:7-30.
8. Gonzalez H, Hagerling C, Werb Z. Roles of the immune system in cancer: from tumor initiation to metastatic progression. Genes Dev 2018;32:1267-84.
9. Postow MA, Sidlow R, Hellmann MD. Immune-Related Adverse Events Associated with Immune Checkpoint Blockade. N Engl J Med 2018;378:158-68.
10. Carosella ED, Ploussard G, LeMaoult J, et al. A Systematic Review of Immunotherapy in Urologic Cancer: Evolving Roles for Targeting of CTLA-4, PD-1/PD-L1, and HLA-G. Eur Urol 2015;68:267-79.
11. Tan G, Xuan Z, Li Z, et al. The critical role of BAP1

mutation in the prognosis and treatment selection of kidney renal clear cell carcinoma. Transl Androl Urol 2020;9:1725-34.
12. Cozma A, Sporis ND, Lazar AL, et al. Cardiac Toxicity Associated with Immune Checkpoint Inhibitors: A Systematic Review. Int J Mol Sci 2022;23:10948.
13. Laity JH, Lee BM, Wright PE. Zinc finger proteins: new insights into structural and functional diversity. Curr Opin Struct Biol 2001;11:39-46.
14. Sera T. Zinc-finger-based artificial transcription factors and their applications. Adv Drug Deliv Rev 2009;61:513-26.
15. Yang L, Zhang L, Wu Q, et al. Unbiased screening for transcriptional targets of ZKSCAN3 identifies integrin beta 4 and vascular endothelial growth factor as downstream targets. J Biol Chem 2008;283:35295-304.
16. Yang L, Wang H, Kornblau SM, et al. Evidence of a role for the novel zinc-finger transcription factor ZKSCAN3 in modulating Cyclin D2 expression in multiple myeloma. Oncogene 2011;30:1329-40.
17. Zhang X, Jing Y, Qin Y, et al. The zinc finger transcription factor ZKSCAN3 promotes prostate cancer cell migration. Int J Biochem Cell Biol 2012;44:1166-73.
18. Jen J, Lin LL, Chen HT, et al. Oncoprotein ZNF322A transcriptionally deregulates alpha-adducin, cyclin D1 and p53 to promote tumor growth and metastasis in lung cancer. Oncogene 2016;35:2357-69.
19. Song J, Nabeel-Shah S, Pu S, et al. Regulation of alternative polyadenylation by the C2H2-zinc-finger protein Sp1. Mol Cell 2022;82:3135-3150.e9.
20. Gandhi AK, Kang J, Havens CG, et al. Immunomodulatory agents lenalidomide and pomalidomide co-stimulate T cells by inducing degradation of T cell repressors Ikaros and Aiolos via modulation of the E3 ubiquitin ligase complex CRL4(CRBN.). Br J Haematol 2014;164:811-21.
21. Licht JD, Shortt J, Johnstone R. From anecdote to targeted therapy: the curious case of thalidomide in multiple myeloma. Cancer Cell 2014;25:9-11.
22. Wang X, Yao L, Li Z, et al. ZNF471 Interacts with BANP to Reduce Tumour Malignancy by Inactivating PI3K/AKT/mTOR Signalling but is Frequently Silenced by Aberrant Promoter Methylation in Renal Cell Carcinoma. Int J Biol Sci 2024;20:643-63.
23. Lu HY, Sertori R, Contreras AV, et al. A Novel Germline Heterozygous BCL11B Variant Causing Severe Atopic Disease and Immune Dysregulation. Front Immunol 2021;12:788278.
24. Chu J, Jiang J, Fan X, et al. A novel MYC-ZNF706-SLC7A11 regulatory circuit contributes to cancer progression and redox balance in human hepatocellular carcinoma. Cell Death Differ 2024;31:1333-48.
25. Kapranov P, Cheng J, Dike S, et al. RNA maps reveal new RNA classes and a possible function for pervasive transcription. Science 2007;316:1484-8.
26. Gibb EA, Brown CJ, Lam WL. The functional role of long non-coding RNA in human carcinomas. Mol Cancer 2011;10:38.
27. Ye ZH, Gui DW, Wang XY, et al. LncRNA SNHG1 promotes renal cell carcinoma progression through regulation of HMGA2 via sponging miR-103a. J Clin Lab Anal 2022;36:e24422.
28. Hu G, Ma J, Zhang J, et al. Hypoxia-induced lncHILAR promotes renal cancer metastasis via ceRNA for the miR-613/206/ 1-1-3p/Jagged-1/Notch/CXCR4 signaling pathway. Mol Ther 2021;29:2979-94.
29. Liu Y, Li X, Zhang C, et al. LINC00973 is involved in cancer immune suppression through positive regulation of Siglec-15 in clear-cell renal cell carcinoma. Cancer Sci 2020;111:3693-704.
30. Li W, Gao LN, Song PP, et al. Development and validation of a RNA binding protein-associated prognostic model for lung adenocarcinoma. Aging (Albany NY) 2020;12:3558-73.
31. Kim S, Kang D, Huo Z, et al. Meta-analytic principal component analysis in integrative omics application. Bioinformatics 2018;34:1321-8.
32. Li Z, Safo SE, Long Q. Incorporating biological information in sparse principal component analysis with application to genomic data. BMC Bioinformatics 2017;18:332.
33. Heagerty PJ, Zheng Y. Survival model predictive accuracy and ROC curves. Biometrics 2005;61:92-105.
34. Iorio F, Knijnenburg TA, Vis DJ, et al. A Landscape of Pharmacogenomic Interactions in Cancer. Cell 2016;166:740-54.
35. Maeser D, Gruener RF, Huang RS. oncoPredict: an R package for predicting in vivo or cancer patient drug response and biomarkers from cell line screening data. Brief Bioinform 2021;22:bbab260.
36. Rooney MS, Shukla SA, Wu CJ, et al. Molecular and genetic properties of tumors associated with local immune cytolytic activity. Cell 2015;160:48-61.
37. Hsieh JJ, Purdue MP, Signoretti S, et al. Renal cell carcinoma. Nat Rev Dis Primers 2017;3:17009.
38. Tamayo P, Cho YJ, Tsherniak A, et al. Predicting relapse in patients with medulloblastoma by integrating evidence from clinical and genomic features. J Clin Oncol

 

2011;29:1415-23.
39. Ahmed AA, Abedalthagafi M. Cancer diagnostics: The journey from histomorphology to molecular profiling. Oncotarget 2016;7:58696-708.
40. Zheng D, Wei Z, Zhang C, et al. ZNF692 promotes osteosarcoma cell proliferation, migration, and invasion through TNK2-mediated activation of the MEK/ERK pathway. Biol Direct 2024;19:28.
41. Singh JK, Smith R, Rother MB, et al. Zinc finger protein ZNF384 is an adaptor of Ku to DNA during classical non-homologous end-joining. Nat Commun 2021;12:6560.
42. Chang J, Zhang Y, Zhou T, et al. RBM10 C761Y mutation induced oncogenic ASPM isoforms and regulated β-catenin signaling in cholangiocarcinoma. J Exp Clin Cancer Res 2024;43:104.
43. Galon J, Bruni D. Tumor Immunology and Tumor Evolution: Intertwined Histories. Immunity 2020;52:55-81.
44. Dunn GP, Bruce AT, Ikeda H, et al. Cancer immunoediting: from immunosurveillance to tumor escape. Nat Immunol 2002;3:991-8.
45. Dunn GP, Old LJ, Schreiber RD. The immunobiology of cancer immunosurveillance and immunoediting. Immunity 2004;21:137-48.
46. La-Beck NM, Jean GW, Huynh C, et al. Immune Checkpoint Inhibitors: New Insights and Current Place in Cancer Therapy. Pharmacotherapy 2015;35:963-76.
47. Zou J, Wang L, Tang H, et al. Ferroptosis in Non-Small Cell Lung Cancer: Progression and Therapeutic Potential on It. Int J Mol Sci 2021;22:13335.
48. Inthagard J, Edwards J, Roseweir AK. Immunotherapy: enhancing the efficacy of this promising therapeutic in multiple cancers. Clin Sci (Lond) 2019;133:181-93.
49. Resch I, Bruchbacher A, Franke J, et al. Outcome of immune checkpoint inhibitors in metastatic renal cell carcinoma across different treatment lines. ESMO Open 2021;6:100122.
50. Liu H, Ye T, Yang X, et al. A Panel of Four-lncRNA Signature as a Potential Biomarker for Predicting Survival in Clear Cell Renal Cell Carcinoma. J Cancer 2020;11:4274-83.
51. Grivennikov SI, Greten FR, Karin M. Immunity, inflammation, and cancer. Cell 2010;140:883-99.
52. Gardner A, Ruffell B. Dendritic Cells and Cancer Immunity. Trends Immunol 2016;37:855-65.
53. Saliby RM, El Zarif T, Bakouny Z, et al. Circulating and Intratumoral Immune Determinants of Response to Atezolizumab plus Bevacizumab in Patients with Variant Histology or Sarcomatoid Renal Cell Carcinoma. Cancer Immunol Res 2023;11:1114-24.
54. Hou W, Xue M, Shi J, et al. PD-1 topographically defines distinct T cell subpopulations in urothelial cell carcinoma of the bladder and predicts patient survival. Urol Oncol 2020;38:685.e1-685.e10.
55. Liu Z, Zhou Q, Wang Z, et al. Intratumoral TIGIT(+) CD8(+) T-cell infiltration determines poor prognosis and immune evasion in patients with muscle-invasive bladder cancer. J Immunother Cancer 2020;8:e000978.
56. Ryder M, Ghossein RA, Ricarte-Filho JC, et al. Increased density of tumor-associated macrophages is associated with decreased survival in advanced thyroid cancer. Endocr Relat Cancer 2008;15:1069-74.
57. Hellmann MD, Nathanson T, Rizvi H, et al. Genomic Features of Response to Combination Immunotherapy in Patients with Advanced Non-Small-Cell Lung Cancer. Cancer Cell 2018;33:843-852.e4.

(English Language Editor: L. Huleatt)

**Cite this article as:** Tian T, Shen C, Zapała Ł, Fang X, Zheng B. Identification of a C2H2 zinc finger-related lncRNA prognostic signature and its association with the immune microenvironment in clear cell renal cell carcinoma. Transl Androl Urol 2025;14(2):412-431. doi: 10.21037/tau-2024-769

 